Babes-Bolyai University
Faculty of Physics

Doctoral Thesis Summary

MULTIFUNCTIONAL PLASMONIC NANOPARTICLES FOR OPTICAL IMAGING AND DETECTION METHODS

Ana-Maria GĂBUDEAN

Scientific advisor
Prof. Univ. Dr. Simion AŞTILEAN

CLUJ-NAPOCA
2012

TABLE OF CONTENT

OUTLINE OF THE THESIS

Chapter 1 provides an overview of the field of gold nanoparticles (AuNPs), their optical properties and most important plasmonic effect emerging from their interaction with light: Surface-Enhanced Raman Scattering (SERS) and Metal Enhanced Fluorescence (MEF). Additionally, some of the most important biomedical applications of AuNPs are being reviewed.

The subsequent three chapters contain results obtained in the Nanobiophotonics Center of the Interdisciplinary Research Institute in Bio-Nano-Sciences from Babes-Bolyai University.

The work presented in **Chapter 2** is focused on the synthesis and characterization of anisotropic rod-shaped gold nanoparticles (AuNRs) with tunable aspect ratio and different surface coatings. The preparation of cetyltrimethylammonium bromide (CTAB)-stabilized AuNRs with tunable optical properties and characterization of their optical properties are being described in the first section. Subsequently, in view of improving the surface chemistry, biocompatibility and stability of the as-prepared AuNPs, silica (SiO_2) and polystyrene sulfonate (PSS) were tested as coating materials. After describing the encapsulation process we characterize optically and morphologically the as- prepared coated-AuNRs.

Chapter 3 emphasizes the appealing properties of CTAB-coated gold nanorods (AuNRs) in view of two relevant sensing applications. As first application, we lay out the study of the interaction between para-aminothiophenol (pATP) Raman tag and CTAB-coated AuNRs as function of pATP molecular concentration and pH values in solution through localized surface plasmon resonance (LSPR) and surface-enhanced Raman scattering (SERS) spectroscopies. We correlate the experimental results with Finite-Difference Time-Domain (FDTD) theoretical data in order to understand the origin of SERS. Additionally, we address the intriguing case that has recently emerged in SERS literature regarding the formation of p,p'-dimercaptoazobenzene (DMAB) through chemical transformation of pATP on metallic substrates by investigating the pH and time-dependent behavior of this process.

The second important application of CTAB-coated AuNRs detailed in this chapter is their ability to perform as efficient plasmonic platforms for the fabrication of dual-responsive spectroscopic nanoprobes. Specifically, we demonstrate the preparation of CTAB-coated AuNRs decorated with Rose Bengal (RB) fluorophore able to operate via both SERS and metal enhanced fluorescence (MEF). We show that the selective excitation of the two surface plasmon resonances of AuNRs can trigger either the enhancement of fluorescence emission or Raman scattering. Moreover, we demonstrate that the resonant excitation of both RB and AuNRs allows the simultaneous detection of surface-enhanced resonance Raman scattering (SERRS) and metal enhanced fluorescence (MEF) signals. To our knowledge, this work represents the first demonstration of fluorophore-encoded AuNRs able to provide a dual-modal enhanced spectroscopic signal via SERS and MEF.

Subsequently, in **Chapter 4** we highlight the potential use of silica (SiO_2)-coated AuNRs in detection applications. In this regard, we first describe the fabrication of two models of spectroscopic tags with near-infrared-SERS signatures based on individual SiO_2-coated AuNRs encoded with pATP, as model of non-fluorescent molecule with strong affinity for gold surface and Nile Blue (NB), a common dye with lower affinity for gold. Additionally, we show that by designing AuNRs with plasmon resonance band overlapping the electronic absorption band of NB, a dual performance of the nanohybrids can be devised under resonant excitation. To our knowledge, this is the first system based on silica-coated AuNRs which exhibits a dual responsive performance through SERRS and MEF simultaneously detected at the same excitation wavelength.

The experimental results presented in the following two chapters were obtained at "Laboratoire interdisciplinaire de Physique", Joseph Fourier University and "Laboratoire de Chimie", Ecole Normale Supérieur de Lyon/Claude Bernard University from France.

The principal goal of **Chapter 5** was to demonstrate the use of optical microspectroscopy as ideal platform for the accurate analyze and characterization of metallic nano-objects. The first section deals with the analysis of newly synthesized hollow gold nanoshells incorporating fluorescent dyes in their liquid cores. We characterize the samples by means of bright field, dark field and fluorescence spectroscopy and microscopy on individual nanoparticles. In the second section, we use fluorescence microscopy-imaging and spectroscopy to demonstrate the luminescence properties of fluorophore-decorated star and bipiramide-shaped AuNPs and discuss the role of the surfactant layer stabilizing the nanoparticles on luminescent performance of the conjugates.

Chapter 6 emphasizes the feasibility of employing surface modified AuNPs in intracellular imaging applications by performing quantitative cellular uptake studies on differently shaped polymer-coated AuNPs. Firstly, we evaluate the cellular uptake of star and bipyramide-shaped AuNPs coated with a layer of thiolated polyethylene glycol by B16-F10 melanoma cells. Secondly, we investigate the interaction of gold nanospheres (AuNSs) encapsulated in newly synthesized polymeric chains with B16-F10 melanoma and BaF3 lymphoid cells as function of colloidal concentration and AuNPs size and assess their potential use in intracellular applications.

This work was supported by "Investing in people" - Ph.D. scholarship, project co-financed by the Sectoral Operational Program for Human Resources Development 2007 – 2013, Contract nr. POSDRU/88/1.5/S/60185 - "Innovative doctoral studies in a knowledge based society", Babeş-Bolyai University, Cluj-Napoca, Romania.

KEYWORDS: gold nanoparticles, Raman tags, fluorescence, MEF, SERS, detection

CHAPTER 1
INTRODUCTION TO GOLD NANOPARTICLES

1.1 Historical background

Although noble metal colloids are considered a discovery of modern science, they have been produced and used way back in ancient times for their remarkable optical properties. They were used in Ancient Roman times to color ceramics and glass intense shades of yellow, red, or mauve, depending on the concentration of gold, and in Hindu Chemistry, for various potions. The first and most famous example is the Lycurgus roman cup from the 4th century BC which turns ruby-red in transmitted light and green in reflected light due to the presence of gold nanoparticles (AuNPs) (see Figure 1-1).

Figure 1-1 The Lycurgus roman cup which appears green in reflected light (left) and ruby-red in transmitted light (right) due to the presence of gold nanoparticles.

1.2 Optical properties of Gold Nanoparticles

The most insightful optical property of AuNPs relies is the so called *surface plasmons* (SP) defined as collective oscillation of free conduction electrons under resonant light excitation. The amplitude of the oscillation reaches maximum at a specific frequency, giving rise to a prominent *surface plasmon resonance* (SPR) band in the optical absorption spectrum of AuNPs. The most popular theory for describing the interaction of oscillating electromagnetic field with nanoparticles of smaller size that the incident light wavelength is the one developed by Mie (Mie, 1908). As demonstrated in a wide range of literature reports, the SPR band intensity, wavelength and bandwidth strongly depends on the metal type, particle size, shape, structure, composition and the dielectric constant of the surrounding medium.

1.3 Plasmonic effects induced by Gold Nanoparticles

This intense electromagnetic field generated by the SPR of AuNPs is able to enhance the fluorescence and Raman signal of molecule situated at their surface or in close proximity.

The Raman scattering arises from the interaction of photons with the electric dipole of a molecule and it has been long been regarded as a valuable spectroscopic tool for the identification of biological and chemical samples as well as for the elucidation of molecular structure, surface processes and interface reactions. The phenomenon in which the Raman scattering intensity from molecules close to metallic surfaces is very much increased is referred to as surface-enhanced Raman scattering (SERS). Although several models have been proposed in the literature, nowadays, two mechanisms are accepted (Campion, 1998): the electromagnetic and the chemical one.

When fluorophores are placed in close proximity to metallic NPs possessing strong plasmon fields, the electrons of the fluorophores participating in the excitation/emission interact with the field, causing the quenching or enhancement of fluorescence. The effect of fluorescence enhancement has been intensively studied by Lakowicz and collaborators over the past decade (Lakowicz, 2006). Briefly, in the proximity of metals, the fluorophore radiative properties are modified and an increase in the spontaneous emission rate is observed which is associated with concomitant increase in the radiative quantum efficiency. This results from the shortening of the fluorescence lifetime, which enables faster cycling of the fluorophore.

1.4 Gold Nanoparticles for Biomedicine

The field of AuNPs has shown fast development over the past decades. They have proven potential use in an ever-growing number of biomedical applications including drug delivery, detection, biological imaging, biosensing, clinical diagnosis and therapy of cancer (Tiwari, 2011). AuNPs are an obvious choice for bio-assays due to their small size to volume ratio, extensive chemical and thermal stability, amenability of synthesis and little toxicity as well as possibility of suitable functionalization with biological molecules.

CHAPTER 2

SYNTHESIS OF GOLD NANORODS WITH DIFFERENT SURFACE COATINGS

The first goal of this chapter was to synthesize cetyltrimethylammonium bromide (CTAB)-stabilized anisotropic rod-shaped nanoparticles with tunable aspect ratio. Secondly, two different coating materials (silica (SiO_2) and polystyrene sulfonate (PSS)) were tested in view of improving the stability, sensibility and biocompatibility of gold nanorods (AuNRs).

The possibility of broadly tuning their optical, catalytic and electronic properties of AuNPs by controlling their size, shape and composition has resulted in a wide number of publications on synthetic methodologies for the preparation of AuNPs with various sizes and shapes from spheres (Shankar, 2005), rods (Huang, 2009), bipyramides (Navarro, 2012), triangles and cubes (Huang, 2006) to stars (Nehl, 2006) and flower (Boca, 2011). In particular, much of the focus has been devoted to gold nanorods (AuNRs) over the last decades due to the relative simple fabrication procedures and control over their aspect ratios. Moreover, in order to improve the properties CTAB-coated AuNRs such as increasing their stability by preventing the aggregation and improving their sensibility and specificity, different coating strategies have been approached.

2.1 Cetyltrimethylammonium bromide (CTAB) - coated Gold Nanorods

2.1.1 Introduction

The two-step seed-mediated growth protocol is the most popular method used for the fabrication in aqueous solution of AuNRs with well defined shape and uniform size. Briefly, this method involves in the first step, the preparation of small gold spherical seeds from gold salt ($HAuCl_4$) and a strong reducing agent able to promote isotropic growth. The second step implies the addition of gold seeds to a growing solution containing additional gold salt, a mild reducing agent and a "structure-directing agent" which aids the anisotropic growth.

We present here the high-yield and size-controlled synthesis of CTAB-coated AuNRs by using the seed -mediated silver ions-assisted two-step wet chemical protocol. We characterize the optical properties of AuNRs by localized surface plasmon resonance (LSPR) spectroscopy and evaluate the morphology of the samples through transmission electron microscopy (TEM).

2.1.2 Localized surface plasmon resonance (LSPR) spectroscopy results

Figure 2-1 shows the normalized extinction spectra of AuNRs with different aspect ratios and the photograph pictures of the corresponding colloidal dispersions in water.

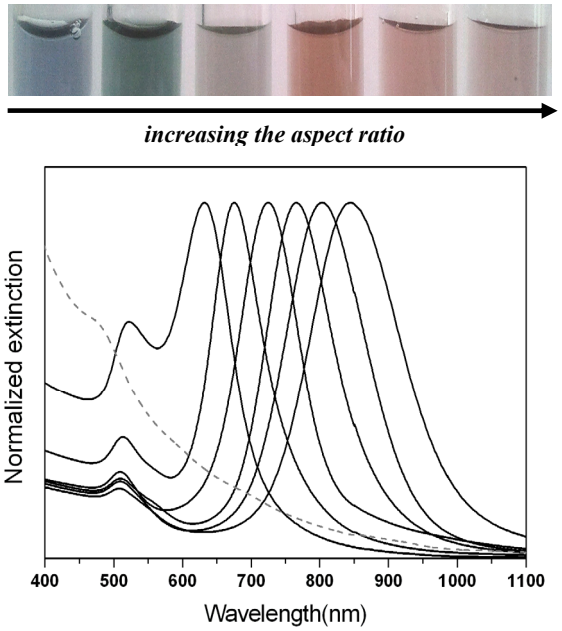

Figure 2-1 Photograph images and normalized extinction spectra of AuNRs with varying aspect ratio in aqueous solution. Dashed line represents the extinction spectrum of the seed solution.

The spectral position of transversal surface plasmon resonances at approximately 513 nm and the large tunability of longitudinal surface plasmon resonance from 630 nm to 840 nm are correlated with their aspect ratios ranging from 2.2 to 4.4.

The color of each batch of AuNRs in aqueous suspension is strongly correlated to their optical response transposed in the spectral position of the longitudinal plasmon resonance.

2.1.3 Transmission electron microscopy (TEM) results

TEM imaging was employed in our study in order to confirm the formation of rod shaped nanoparticles and moreover, to estimate their dimensions and aspect ratios. Figure 2-2 presents high-magnification TEM images of three different aspect ratio synthesized AuNRs. The analyzed nanoparticles appear as rod-shaped individual entities with a good monodispersity in shape and size. The average length × width dimensions obtained the randomly chosen aspect ratios of 2.3, 3.4 and 4 are: 41.5 × 18 nm, 37.5 × 11 nm and 44 × 11 nm.

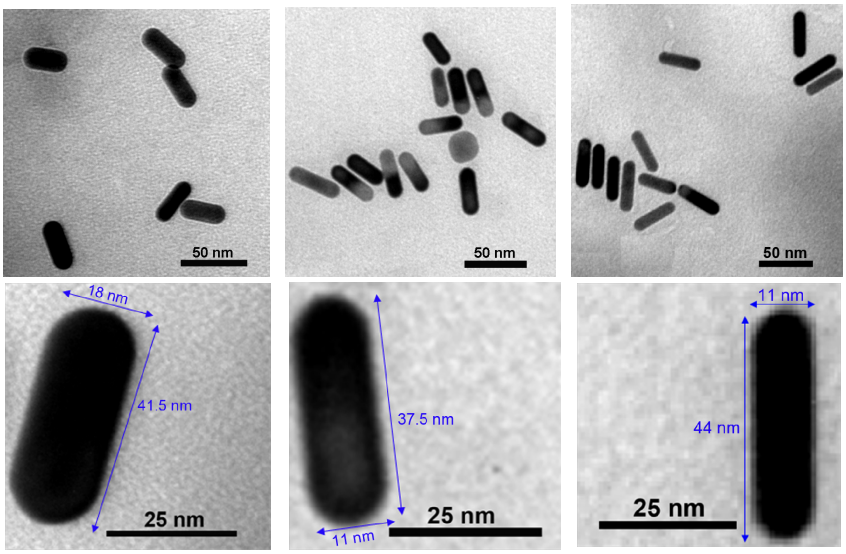

Figure 2-2 Illustrative high-magnification TEM images of AuNRs with different aspect ratios: 2.3, 3.4 and 4.

2.2 Silica - encapsulated Gold Nanorods

2.2.1 Introduction

The current stategy of coating nanoparticles with protective layers of biocompatible materials (e.g. silica(SiO_2)) for improved stability and inertness, allows the preparation of suitable probes for biomedical investigations.

In this section, we demonstrate the successful encapsulation of AuNRs with mesoporous SiO_2 shells by a simple one-step method based on the condensation of tetraehylorthosilicate (TEOS) in a seeded growth process. The encapsulation of AuNRs in SiO_2 is experimentally confirmed by localized surface plasmon resonance (LSPR) spectroscopy, transmission electron microscopy (TEM), dynamic light scattering (DLS) and Zeta Potential measurements.

2.2.2 Localized surface plasmon resonance (LSPR) spectroscopy results

The encapsulation procedure was performed on different aspect ratio CTAB-coated AuNRs. Specifically, we have selected CTAB-coated AuNRs with longitudinal LSPR bands centered at 640, 675, 760 and 805 nm, respectively, further denoted as $AuNRs_{640}$, $AuNRs_{675}$, $AuNRs_{760}$ and $AuNRs_{805}$. As a direct consequence of the SiO_2 layer deposition, the longitudinal LSPR resonances undergo significant shifts toward longer wavelengths due to the increase of local refractive index in the close proximity of metal surface (see Figure 2-3).

The variable LSPR red-shifts between 7 and 20 nm indicate the formation of silica shell of different thicknesses.

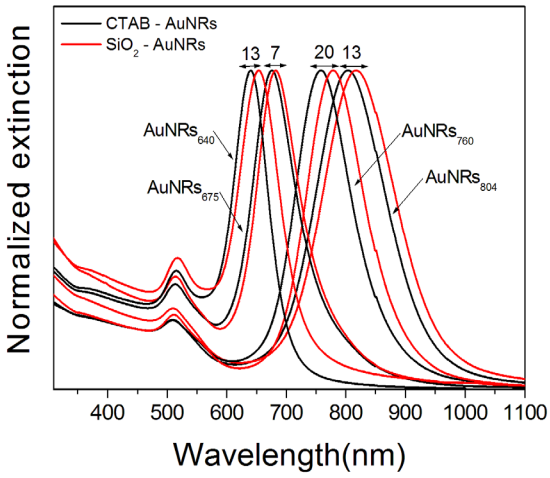

Figure 2-3 The normalized extinction spectra of different aspect ratio AuNRs before and after coating with silica. The four types of samples are denoted: $AuNRs_{640,}$ $AuNRs_{675}$, $AuNRs_{760}$ and $AuNRs_{805}$.

2.2.3 Transmission electron microscopy (TEM) results

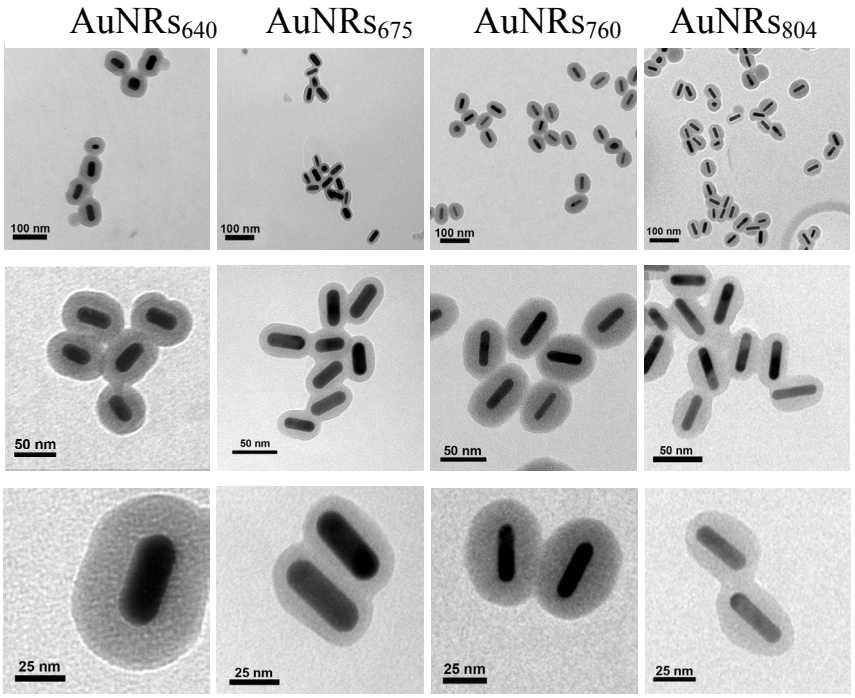

Figure 2-4 Illustrative low and high-magnification TEM images of AuNRs after encapsulation in silica. From top to bottom, we exemplify three representative TEM images for each of the different aspect ratio samples: $AuNRs_{640,}$ $AuNRs_{675}$, $AuNRs_{760}$ and $AuNRs_{805}$

Figure 2-4 shows representative TEM images of $AuNRs_{640,}$ $AuNRs_{675}$, $AuNRs_{760}$ and $AuNRs_{805}$, respectively, after coating with SiO_2. As illustrated, the silica layers are clearly visible around the AuNRs as grey contrasting shells of varying thicknesses. We noticed that increasing the thickness of the SiO_2 layer produces the increase of plasmon resonance red-shift. For example, the largest red-shift of 20 nm observed for the $AuNRs_{760}$ is perfectly matched with the thickest SiO_2 layer formed at the surface of as-prepared CTAB-coated AuNRs that is the 20±2 nm layer identified in the case of sample $AuNRs_{760.}$

CHAPTER 3

APPLICATIONS OF CTAB-COATED GOLD NANORODS

3.1 Localized surface plasmon resonance (LSPR) and surface-enhanced Raman scattering (SERS) studies of para-aminothiophenol adsorption on gold nanorods

Here, we exploit the optical properties of AuNRs with the aim of investigating by LSPR and SERS the adsorption of para-aminothiophenol (p-ATP) molecules as function of molecular concentration and pH values in solution. Finite-Difference Time-Domain (FDTD) simulations were used to evaluate the electromagnetic field distribution at the surface of individual and end-to-end assembled AuNRs. Additionally, we addressed an intriguing case that has recently emerged in SERS literature regarding the interpretation of p,p'-dimercaptoazobenzene (DMAB) molecule SERS spectrum, formed through coupling of p-ATP molecules.

3.1.1 Analysis of concentration-dependent LSPR/SERS spectra

We first investigated the optical response of p-ATP/AuNRs conjugates as a function of analyte concentration. Figure 3-1A shows the LSPR spectra of ten samples prepared by mixing 1 ml AuNRs solution at pH=7 with 25 µl p-ATP solution of different concentrations. The spectra reveal the steady decrease of intensity and shift of longitudinal LSPR band as function of increasing p-ATP concentration. The LSPR spectral red-shift gradually decreases with increasing concentration (see Figure 3-1B), effect which can be explained as interplay between two events, namely the binding of p-ATP and desorption of CTAB layer from the surface of AuNRs.

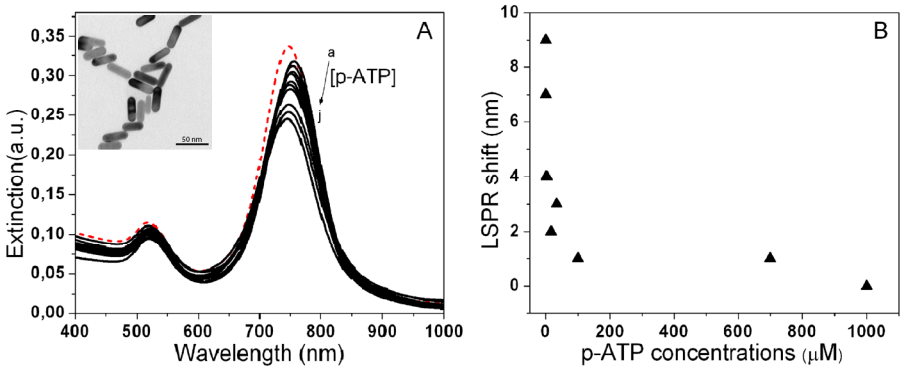

Figure 3-1 (A) Extinction spectra of p-ATP coated AuNRs in solution, recorded at varying p-ATP concentration ranging from 0.034 μM to 1 mM (a-j). (B) Longitudinal plasmon band shift as a function of p-ATP concentration.

As illustrated in Figure 3-2A, the SERS signal of p-ATP systematically increases as the concentration increases. The SERS spectra are dominated by the a_1 modes at 1079 cm^{-1} and 1585 cm^{-1} attributed to C-S and C-C stretching vibrations. A saturated monolayer adsorption of p-ATP is reached when the concentration of p-ATP is >100 μM, a result which correlates with the limit of concentration which is detectable LSPR (see Figure 3-1B). By interpolating the experimental data in Figure 3-2B we found the p-ATP adsorption coefficient of $3.55 \cdot 10^{-5}$ M^{-1}.

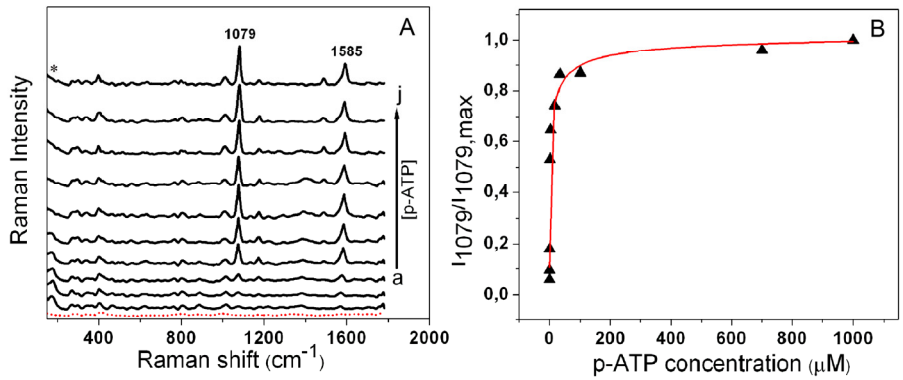

Figure 3-2 (A) SERS spectra of p-ATP coated AuNRs in solution, recorded at varying p-ATP concentration ranging from 0.034 μM to 1 mM (a-j). The dash-dotted curves represent the extinction and Raman spectra recorded from pure nanorods solution. (B) Langmuir curve.

3.1.2 Analysis of pH-dependent LSPR/SERS spectra

We further investigated the LSPR and SERS sensitivity of p-ATP/AuNRs conjugates to a local change in pH. Specifically, at pH=11 we detect a significant decrease in intensity of the longitudinal plasmon resonance along with a broadening of the band over a large region from the

NIR-IR domain, indicating the formation of end-to-end assemblies of AuNRs with thiolic molecules trapped between coupled AuNRs, as supported by TEM imaging (Figure 3-3 A, B).

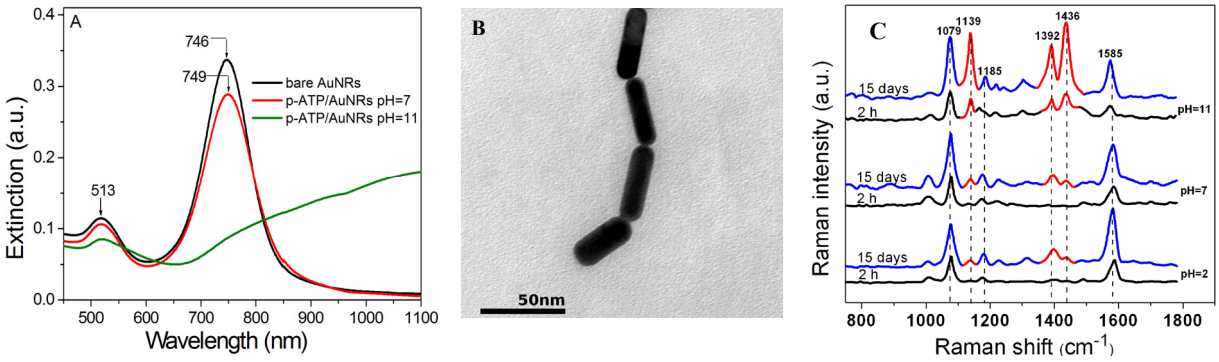

Figure 3-3 (A) Extinction spectra of bare AuNRs and p-ATP/AuNRs conjugates (p-ATP concentration 24 μM) in solution at two different pH values, (B) Representative TEM image of p-ATP/AuNRs at pH=11 and (C) SERS spectra of p-ATP/AuNRs conjugates in solution at three different pH values, recorded 2h (i) and 15 days (ii). Excitation: 785 nm laser line.

As displayed in Figure 3-3C, the SERS spectrum of conjugates at pH~11 displays along with the a_1 modes, three new peaks at 1139, 1392 and 1436 cm^{-1}, which can be assigned to the formation of p,p'-dimercaptoazobenzene (DMAB) molecule by catalytic coupling reaction of p-ATP. Figure 3-4 shows the distribution of relative intensity of the electromagnetic field at the surface of individual and end-to-end coupled AuNRs at the wavelength of 785 nm, according to the laser line used in SERS experiments.

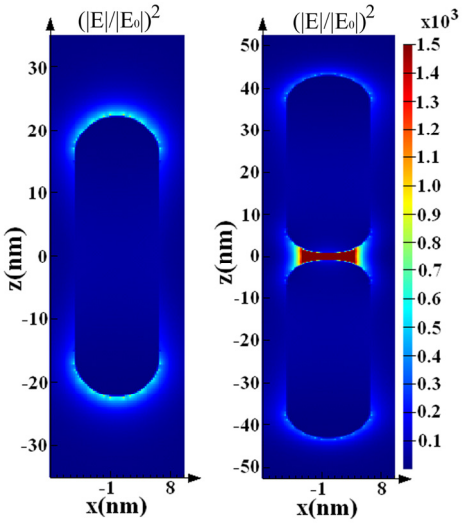

Figure 3-4 Electric-field enhancement at the surface of AuNRs at the excitation laser line of 785 nm: (left) individual and (right) end-to-end coupled AuNRs of 42.5 nm length and 12.5 nm width according to TEM.

In the case of end to-end coupling a much higher electric field is induced in the gap between AuNRs, due to plasmonic coupling between NPs, which results in the largest Raman scattering enhancements for molecules residing in the gap, giving so-called SERS ‘‘hot spots”.

3.2 Gold Nanorods Performing as Dual-Modal Nanoprobes via Metal-Enhanced Fluorescence (MEF) and Surface-Enhanced Raman Scattering (SERS)

We report the successful fabrication of a dual-responsive plasmonic platform based on CTAB-coated AuNRs decorated with Rose Bengal (RB) fluorophore. While the CTAB layer captures RB molecules preventing fluorescence quenching, the selective excitation of the two surface plasmon resonances of AuNRs can trigger either the enhancement of fluorescence emission or Raman scattering. Moreover, we demonstrate that the resonant excitation of both RB and AuNRs allows the simultaneous detection of surface-enhanced resonance Raman scattering (SERRS) and metal enhanced fluorescence (MEF) signals.

3.2.1 MEF characterization

In this work the premise of fluorescence enhancement is provided by the fact that the CTAB layer can play both the role of spacer and linker by fixing the RB molecules at about 4 nm far from the metal surface (Yu, 2007) as schematically shown in Figure 3-5A.

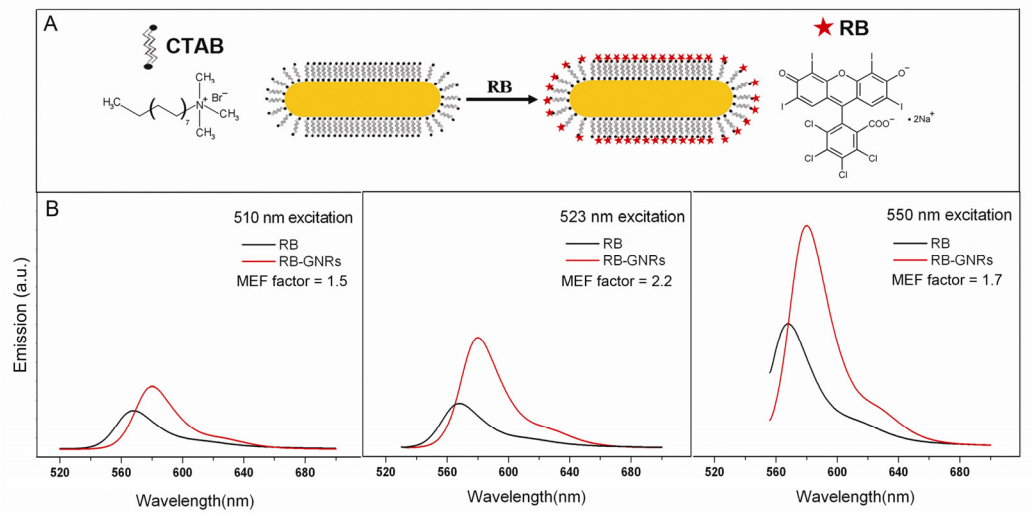

Figure 3-5 (A) Schematic diagram illustrating the labeling of CTAB-coated AuNRs with RB. (B) Emission spectra of RB-AuNRs conjugates together with the emission of free RB in water as recorded for three excitation wavelengths at 510, 523 and 550 nm.

Regardless the excitation wavelength, the fluorescence spectra collected from RB-AuNRs are enhanced relative to the fluorescence spectra collected from free RB. The biggest enhancement of 2.2-fold was observed when both RB and AuNRs in RB-AuNRs conjugates transversal plasmon resonance band are resonantly excited at 523 nm. We admit that the overall enhancement of fluorescence combines effects based on both MEF mechanisms, *i.e*. an increase of the radiative emission rate when nanorods behave as effective optical nanoantennas and an increase of excitation rate in the case of resonant excitation of surface plasmons (Bharadwaj, 2009). The increase of radiative rate of RB molecules in the presence AuNRs is consistent with the decrease of fluorescence lifetime. Thus, we examine the photostability of RB in RB-GNRs by recording the steady-state emission intensity under continuous resonant laser irradiation. As shown in Figure 3-6 the free RB fluorophores undergo a significantly faster photobleaching as compared to the RB immobilized onto AuNRs, indicating that the photostability of fluorophore was extended onto the metal particles in agreement with the average enhancement factor. The decrease of photobleaching probabiblity demonstrates indirectly the reduction of fluorophore lifetime and, implicitly, the contribution of quantum efficiency increase (i.e. radiative rate) in MEF.

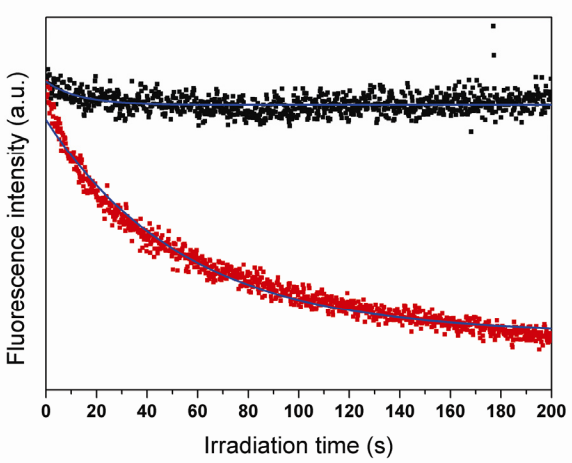

Figure 3-6 Photobleaching rate of RB-AuNRs conjugates (black dots) as compared to that of free RB (red dots) upon high-intensity irradiation at 532 nm.

3.2.2 SERS characterization

Figure 3-7 shows for comparison the spectra recorded from RB-AuNRs conjugates and from free RB molecules in solution.

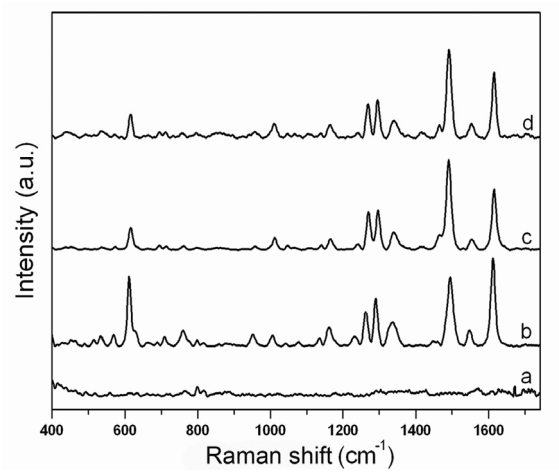

Figure 3-7 Normal Raman and SERS spectra: (a) free RB in solution of 10^{-6} M, (b) SERS spectrum of RB in RB-AuNRs conjugates of 10^{-6} M concentration, (c) free RB in solution of 5×10^{-2} M, (d) RB-CTAB conjugates in solution of 5×10^{-2} M. Excitation: 785 nm laser line

The band assignment was performed on the basis of published data on RB and related xanthenes molecules (Narayanan, 1994; Maciejewska, 1993; Vosgrçne, 2005). We note the relative enhancement of C-I and C-Cl vibrational bands at 611 cm^{-1} and 760 cm^{-1}, as well as the enhancement and modification of the ratio between the intensities of ν_{as}(C=C) and ν_s(C=C) vibrational bands at 1495 cm^{-1} and 1612 cm^{-1}, suggesting the orientation of RB molecule with respect to metal surface such that the $-O^-$ and $-COO^-$ groups of RB point toward $(CH_3)_3N^+$ group in CTAB. By taking as reference band the vibration from 611 cm^{-1}, we found an experimental average EF of 1.7×10^5.

3.2.3 Multiplexed response

RB-AuNRs conjugates can enhance simultaneously the Raman and fluorescence signal when excited at specific laser lines. The excitation at 785 nm laser line, far away from the electronic absorption band of RB, produces only a normal SERS signal as previously demonstrated. However, when RB-AuNRs conjugates are excited at 532 nm laser line which is in resonance with both the electronic absorption band of fluorophore and plasmon resonance of substrate, surface-enhanced resonance Raman scattering (SERRS) and MEF can be detected together. Under typical SERRS conditions the fluorescence is usually quenched by metal, contrary to our case where the fluorophore was intentionally placed at distance from the metal.

Figure 3-8 shows the spectrum recorded from RB-AuNRs conjugates excited at 532 nm laser line at intensity well below saturation (spectrum a).

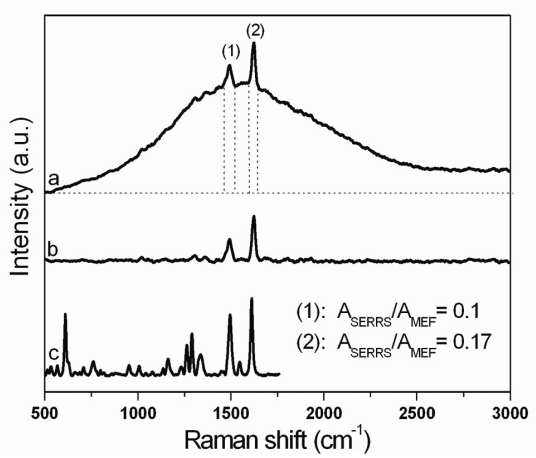

Figure 3-8 MEF and SERRS spectra of RB-AuNRs conjugates: (a) overlapped MEF and SERRS spectra (b) SERRS spectrum after fluorescence background subtraction (c) SERS spectrum as recorded at 785 nm laser line.

Finally, with the aim to demonstrate the potential of CTAB-coated AuNRs to operate as multiplexed SERS nanoprobes, we labeled the RB-AuNRs conjugates with a second, non-fluorescent SERS-active tag, namely pATP. The SERS spectrum recorded from pATP-RB-AuNRs conjugates in solution displays the Raman fingerprints of the two molecules (Figure 3-9 spectrum c) as compared to the reference spectra recorded for the pATP-AuNRs and RB-AuNRs conjugates (Figure 3-9 spectra a and b).

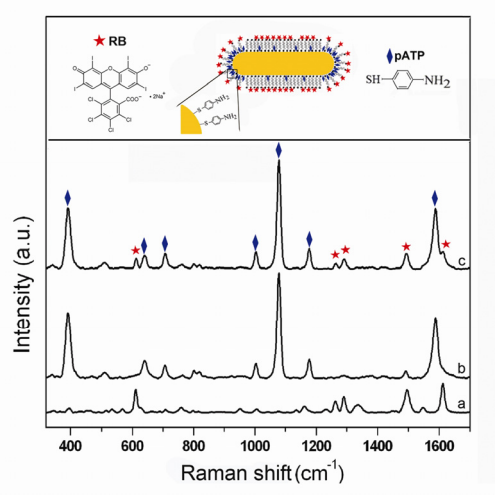

Figure 3-9 SERS spectra of: (a) RB-AuNRs, (b) pATP-AuNRs and (c) pATP-RB-AuNRs nanoconjugates in solution. Excitation: 785 nm laser line.

CHAPTER 4

SILICA-ENCAPSULATED GOLD NANORODS AS EFFICIENT HYBRID PLASMONIC PLATFORMS

In this chapter we discuss the successful fabrication of SiO_2-coated gold nanorods (AuNRs) encoded with two molecular labels as highly effective spectroscopic nano-tags in near-infrared surface-enhanced Raman-scattering SERS (NIR-SERS). Additionally, as result of designing AuNRs with plasmon resonance band overlapping the absorption band of the Nile Blue Raman tag, a dual SERRS and MEF performance has been devised under resonant excitation.

4.1 NIR-SERS-active substrates

p-ATP was the first Raman reporter chosen for the labeling of AuNRs with an aspect ratio of 2.7 and corresponding longitudinal LSPR band centered at 676 nm. After incubation with p-ATP, a batochromic shift of 3 nm is detected for the longitudinal plasmonic band, indicating that pATP thiolic molecules are preferentially attached to the more exposed free ends of AuNRs. As a direct consequence of the SiO_2 layer deposition at the surface of AuNRs, the longitudinal band undergoes a significant 15 nm red–shift along with relative important spectral broadening (see Figure 4-1 (left) – curve c). The silica layer is visible in the TEM image as an approximate 9 nm thick layer surrounding the AuNRs.

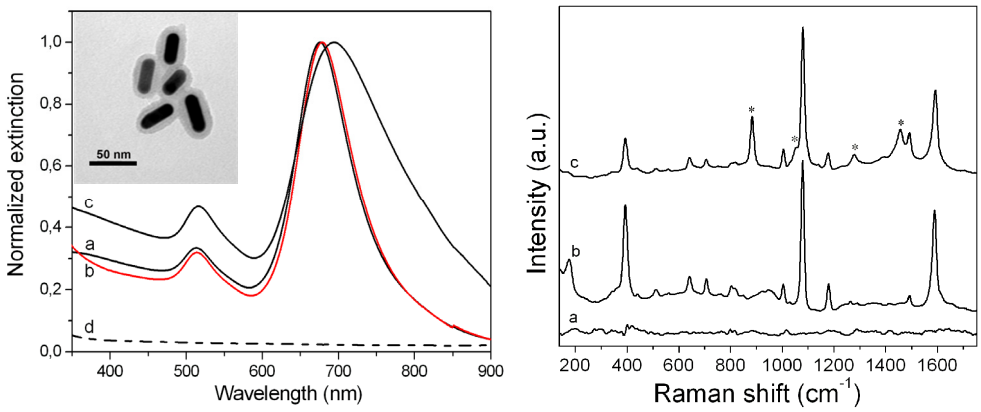

Figure 4-1 (Left): Normalized extinction spectra of raw AuNRs (a) and p-ATP/AuNRs conjugates before (b) and after (c) coating with SiO_2; (d) free p-ATP(10^{-5} M) in water solution; Inset: TEM image. **(**Right**)** (a) Normal Raman spectra recorded from a 10^{-5} M free p-ATP solution and SERS spectra of (b) p-ATP/AuNRs conjugates and (c) SiO_2-coated p-ATP/AuNRs nanohybrids in solution. * Raman peaks of ethanol. Excitation laser line: 785 nm.

After the successful enveloping of the p-ATP/AuNRs conjugates into a SiO_2 shell, we demonstrate the ability of the as-fabricate platforms to operate as NIR-SERS active substrates. Figure 4-1 (right) shows that the strong emitting p-ATP/AuNRs conjugates retain their SERS activity after encapsulation in SiO_2 when excited with the 785 nm laser line.

Hereinafter, we designed a second NIR-SERS responsive system based on SiO_2-coated AuNRs where the Raman label is Nile Blue (NB), a fluorescent dye with relevant photosensitizing abilities, positively charged in water solution. In order to improve the binding strength of the molecules on gold surface, we adjusted the pH of the solution toward alkaline values leading to the partial deprotonation of positive groups in NB molecule, and weakening of the repulsion with CTAB. The formation of conjugates is demonstrated by the red-shift of the longitudinal plasmon band of AuNRs, while the additional displacement indicates the formation of silica layer. The thickness of the formed shell is about 16 nm, as demonstrated by TEM imaging.

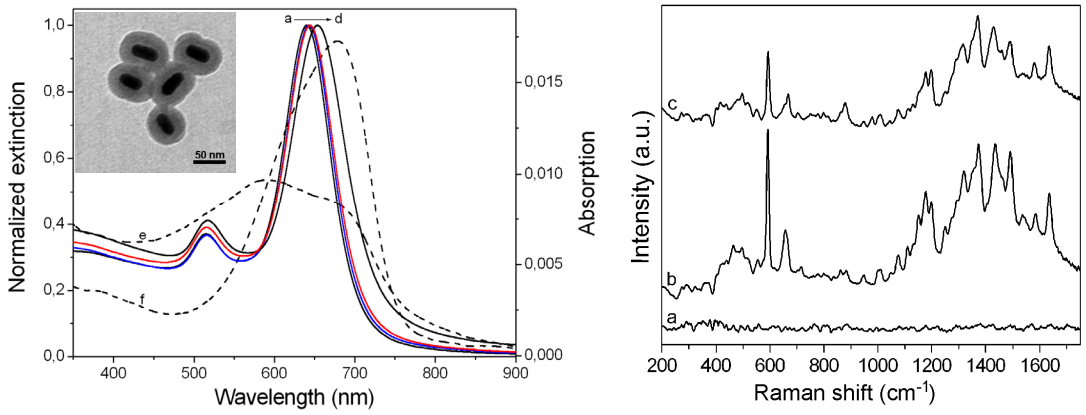

Figure 4-2 (Left) Normalized extinction spectra of: (a) AuNRs, (b) NB/AuNRs at pH=6, (c) NB/AuNRs at pH=10 and (d) SiO_2-coated NB/AuNRs nanohybrids. Absorption spectra of free NB in water solution (1.5×10^{-6} M) at pH=6 (e) and pH=10 (f). Inset: TEM image. (Right) (a) Normal Raman spectra recorded from a 1.5×10^{-6} M free NB solution, (b) SERS spectrum of NB/AuNRs conjugates in solution, at pH 10 and (c) SERS spectrum of SiO_2-coated NB/AuNRs nanohybrids in solution.

In the SERS spectrum of NB/AuNRs conjugates (Figure 4-2 (right) - curve b) a rich spectroscopic signature of NB can be identified, which is well retained after the deposition of a protective SiO_2 layer at the surface of NB/AuNRs conjugates, proving the potential use of the designed nanohybrids as NIR-SERS tags.

4.2 Dual SERRS-MEF substrates

In order to address the challenging task of fabricating biocompatible dual-responsive conjugates with future applicability in biological investigations, we extended our demonstration and investigated the spectroscopic response of SiO_2-coated NB-AuNRs conjugates under resonant excitation, by using the 633 nm laser line. Analyzing the case of NB/AuNRs conjugates, we observe that the fluorescence is only partially quenched by the metallic surface allowing thus the simultaneous detection of fluorescence and SERRS signals under resonant conditions (Figure 4-3, curve a). The multiplexed signature of NB/AuNRs conjugates can still be detected after encapsulation in SiO_2. Despite the obvious decrease in intensity, the most important Raman peaks of NB can still be detected on top of fluorescence signal.

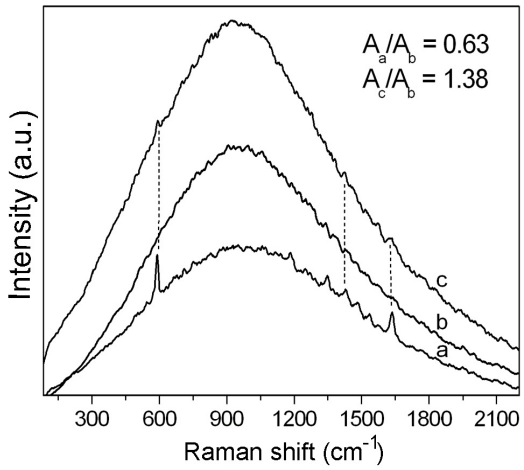

Figure 4-3 Overlapped fluorescence/Raman signals from NB in resonant conditions: (a) fluorescence/SERRS spectrum of NB/AuNRs conjugates at pH=10, (b) fluorescence spectrum of 1.5 x 10^{-6} M NB free NB in water solution at pH=10 and (c) MEF/SERRS spectrum of SiO_2-coated NB/AuNRs nanohybrids. Excitation: 633 nm laser.

CHAPTER 5

INVESTIGATION OF FLUOROPHORE-METAL INTERACTION AT SINGLE NANOPARTICLE LEVEL USING OPTICAL MICROSCOPY AND SPECTROSCOPY

The complex interaction of metallic nano-objects with fluorescent molecules has been intensively addressed over the last few decades as an extremely challenging issue In this context, optical microspectroscopy represents an ideal platform for the accurate analyze and characterization of single fluorescent nanoprobes.

We therefore aim in this chapter to provide a reliable optical characterization of fluorophore-labeled gold nanoparticles through optical microscopy and spectroscopy studies on individual nanoparticles.

5.1 Optical characterization of dye-embedded hollow gold nanoshells

The goal of this study was to explore through optical microscopy and spectroscopy on individual particles the optical properties of an innovative type of nanoparticles consisting in hollow gold nanoshells incorporating fluorescent dyes in their liquid cores. This is a new kind of hybrid nanoshells exhibiting luminescent properties strong enough to be observed and measured for the first time.

The samples optically analyzed were prepared by the chemistry group of the Multimaterials and Interface Laboratory, University Claude Bernard, Lyon. The samples optically characterized consisted in gold nanoshells doped in their liquid cores with a dibromobenzene derivative (DmT) bearing a thioctic unit which allows a direct grafting on gold through sulfur–gold interactions

5.1.1 Light extinction and scattering measurements

As displayed in Figure 5-1, the nanoparticles exhibit a broadband with two resonances in the 600-800 nm spectral region. Specifically, a shoulder resonance can be distinguished around 650 nm together with a second maximum at about 780 nm. According to a generalized version of Mie scattering theory incorporating the higher order multipoles of the scattering expansion (Sarkar, 1997), the peak at 650 nm corresponds to higher order contributions.

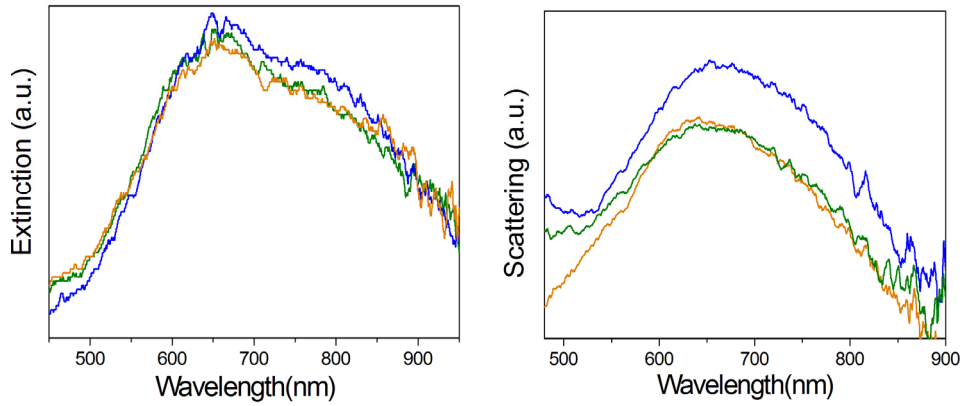

Figure 5-1 Extinction (left) and scattering spectra (right) collected from single DmT@Au nanocapsules redispersed in thin BSA films.

In order to investigate the contribution of light scattering to the total extinction of the nanoparticles we collected the scattering spectra of individual DmT@Au nanocapsules in dark field microscope configuration. After a close inspection, we infer that the light scattering is the

main contribution to the transmission losses, while the absorption process has a much smaller contribution, due to the large size of the nanoparticles.

5.1.2 Fluorescence measurements

The next step in our study was to evaluate the fluorescence properties of the nanocapsules, understand the location of the chromophore and its peculiar interactions with the gold structure. Figure 5-2 shows that this emission band is strongly red shifted in comparison to the emission bands of the DmT molecule in different organic solvents. However, it corresponds to the fluorescence emission wavelength of the solid state fluorescence of DmT powder. Since compound DmT is not soluble in water this result suggests that the chromophore has aggregated and it is in a solid state inside the shell.

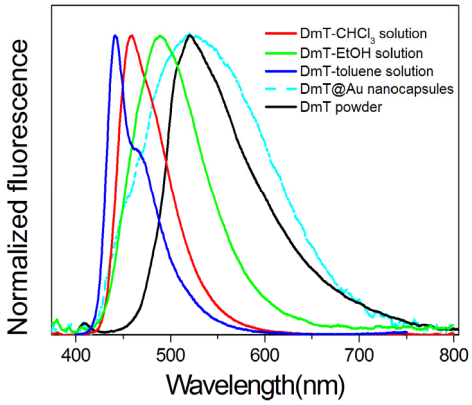

Figure 5-2 Normalized fluorescence emission spectra of compound DmT in powder and in different organic solvents compared to DmT@Au nanocapsules BSA film under excitation at 365 nm.

5.2 Fluorescence microscopy and spectroscopy of gold nanoparticles directly grafted with fluorophore molecules

In this section, we present the successful preparation of fluorophore-decorated star and bipiramide-shaped AuNPs exhibiting strong fluorescence signal confirmed at individual nanoparticle level using fluorescence microscopy-imaging and spectroscopy.

We investigate the direct interaction of Lucifer Yellow Cadaverine (LY), a commercial fluorescent dye used in cell biology with two differently-shaped types of AuNPs: stars and bipyramides. The nanoparticles as well as the fluorescent conjugates were prepared at the Multimaterials and Interface Laboratory, Claude Bernard University, Lyon.

5.2.1 Star-shaped grafted Gold Nanoparticles

Under excitation at 390 nm, in resonance with the main electronic absorption band of LY, the decorated nanoparticles were successfully imaged by epi-fluorescence microscopy as intense bright spots (see Figure 5-3 (Left)). The fluorescence signal emitted by the LY molecules in conjugated state is 15 nm blue shifted compared to the spectrum of LY in free state (see Figure 5-13 B), proving the interaction occurring between the LY and the star-shaped nanoparticles.

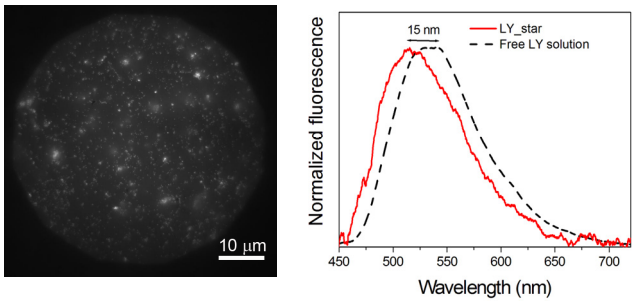

Figure 5-3 (Left) Fluorescence imaging of LY_star conjugates obtained using epi-fluorescence at 390 nm excitation. (Right) Normalized fluorescence emission spectra of LY_star conjugated nanoparticles and free LY molecules in solution. Excitation: 390 nm.

5.2.2 Bipyramide-shaped grafted Gold Nanoparticles

The specific excitation of the LY absorption band with 390 nm light triggers the fluorescence emission of the fluorophore molecules grafted at the surface of bipyramide-shaped gold nanoparticles. Interestingly, individual nanoparticles tend to self-assemble into chain-like nanostructures which emit strong fluorescence light as evidenced by the close-view fluorescence images from Figure 5-4 (Left).

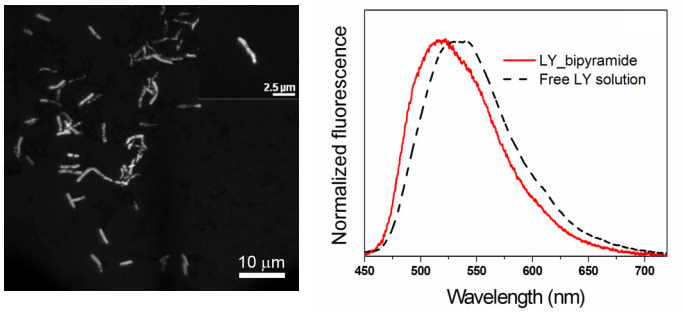

Figure 5-4 (Left) Fluorescence imaging of LY_bipyramide conjugates obtained using epi-fluorescence at 390 nm excitation. (Right) Normalized fluorescence emission spectra of LY_bipyramide conjugated nanoparticles and free LY molecules in solution. Excitation: 390 nm.

After a careful examination of the fluorescent nanostructures we concluded that we have an average number of 10 individual bipyramides per chain. Typical fluorescence emission spectrum recorded from chain-like assembled LY-grafted gold bipyramides is displayed in Figure 5-4 (Right). The fluorescence signal emitted by the LY molecules in conjugated state is 15 nm blue shifted compared to the spectrum of LY in free state in aqueous solution recorded under identical conditions proving the formation of fluorescent conjugates.

CHAPTER 6

CELLULAR UPTAKE STUDIES ON GOLD NANOPARTICLES BY DARK FIELD MICROSCOPY AND SPECTROSCOPY

Despite the certified applicability of gold nanoparticles (AuNPs) in a wide range of biomedical applications, probing their interaction with biomedical systems is a subject of constant interest in the scientific community due to the growing need in modeling them in a more stable, efficient, non-toxic and biological friendly manner.

In this chapter we focus on cellular uptake studies performed on differently shaped polymer-coated gold nanoparticles (AuNPs) by dark-field and contrast phase imaging complemented by light scattering spectroscopy.

We performed cellular uptake studies on two classes of gold nanoparticles (AuNPs): (i) star and bipyramide-shaped AuNPs biocompatibilized through functionalization with a layer of thiolated polyethylene glycol (PEG_{2000}-SH) and (ii) gold nanospheres (AuNSs) encapsulated in a newly synthesized polymer with chain-like structure and a predicted molecular weight of 32200 kDa (32k_polymer), grafted with dye molecule, respectively.

6.1 Cellular uptake assays on PEGylated Gold Nanoparticles

We assessed through dark-field and contrast phase imaging whether the PEGylated AuNPs could be internalized by cancer cells. The melanoma B16-F10 cells without AuNPs show very weak light scattering signal distributed homogeneously within the cell while little bright spots could be detected (Figure 6-1). After incubated for 24 h with ~ 0.5nM PEGylated gold nanostars and bipyramids the cells showed a robust uptake. Dark-field imaging confirms the distribution of AuNPs in vesicles throughout the cytoplasm of the cells. The internalized AuNPs appear as bright shining spots due to their well known ability to scatter strongly the light.

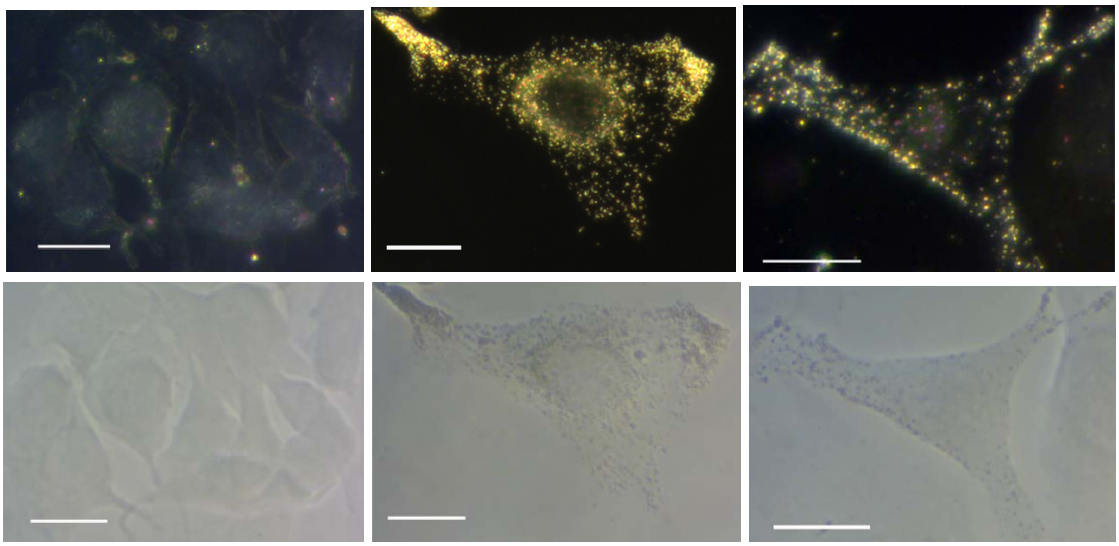

Figure 6-1 Dark-field (top) and contrast phase (bottom) microscopy images of raw melanoma B16-F10 cells (left) and incubated with PEGylated gold nanostars (middle) and bipyramids (right). Scale bars represent: 20 µm.

6.2 Cellular uptake assays on Polymer_32k-coated Gold Nanoparticles

We evaluated the concentration and size-dependent cellular uptake of gold nanospheres (AuNSs) encapsulated in newly synthesized polymeric chains inside B16-F10 melanoma and BaF3 lymphoid cells. Characteristic dark-field images obtained from BaF3 cells incubated in the presence of 70 and 100 nm diameter AuNSs (S70 and S100) coated in polymer_32k are displayed in Figure 6-2. The successful uptake of polymer-coated AuNSs in cells is proven by the presence of intense bright yellow to orange spots throughout the cytoplasm. The extent of scattered light increases with the concentration and the size of AuNPs.

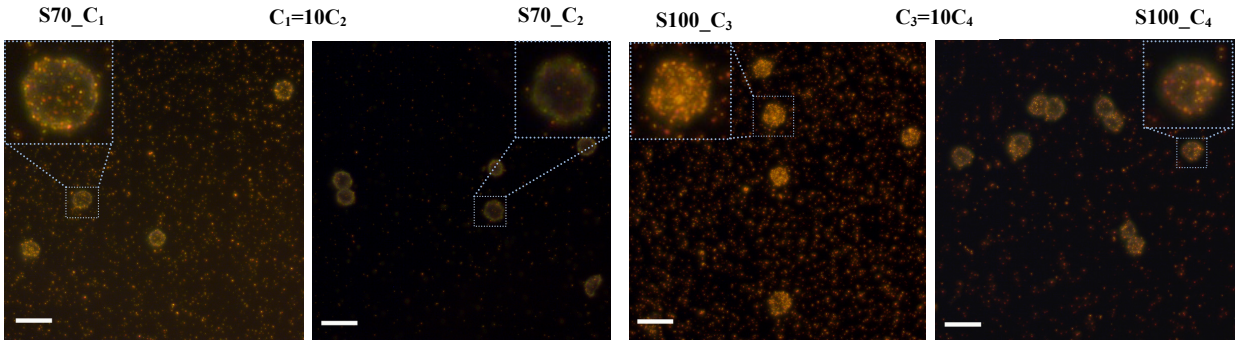

Figure 6-2 Dark-field microscopy images of Baf3 cells incubated with polymer_32k coated AuNSs of 70 nm (left) and 100 nm (right) diameter, respectively. Cellular uptake was tested under two different concentrations for each type of AuNSs, denoted as C_1 and C_2 for S70 and C_3 and C_4 for S100, respectively. All scale bars represent: 20 µm.

CHAPTER 7
FINAL CONCLUSIONS AND PERSPECTIVES

- The first part of my thesis is focused on the synthesis and characterization of anisotropic rod-shaped gold nanoparticles (AuNRs) with tunable aspect ratio and different surface coatings. Cetyltrimethylammonium bromide (CTAB)-stabilized AuNRs were first prepared through a seed mediated growth approach. Afterward, in view of improving their stability and biocompatibility we tested silica (SiO_2) and polystyrene sulfonate (PSS) as coating materials.

  Supplementary future work in this field could involve the optimization of the silica-encapsulation procedure in view tailoring the desired plasmonic response of AuNRs as well as testing other biocompatible materials for the encapsulation of AuNRs.

- We subsequently exploited the optical properties of CTAB-stabilized AuNRs with the aim of studying the adsorption of para-aminothiophenol (pATP) as function of molecular concentration and pH values in solution by localized surface plasmon resonance (LSPR) and surface-enhanced Raman scattering (SERS) spectroscopies. The experimental results were well correlated with Finite-Difference Time-Domain (FDTD) simulation data. Additionally, we brought evidence for the chemical transformation of pATP in p,p'-dimercaptoazobenzene (DMAB) species at elevated pH values.

- Another significant demonstration of my thesis is the fabrication of a dual-responsive plasmonic platform based on CTAB-coated AuNRs decorated with Rose Bengal (RB) fluorophore operating via both SERS and metal enhanced fluorescence (MEF). The CTAB layer on AuNRs prevents fluorescence quenching and optimizes both fluorescence and Raman enhancement, while the simultaneous excitation of RB absorption band and AuNRs plasmon resonance enabled the effective detection of both surface-enhanced resonance Raman-scattering (SERRS) and MEF signals simultaneously. This demonstration represents an original report on the realization of fluorophore-encoded AuNRs able to provide a dual-modal enhanced spectroscopic signal.

- We further reported on the successful fabrication of two models of spectroscopic tags with near-infrared-SERS signatures based on individual SiO_2-coated AuNRs encoded with pATP, as model of non-fluorescent molecule with strong affinity for gold surface and Nile Blue

(NB), a common dye with lower affinity for gold. Additionally, as result of designing AuNRs with plasmon resonance band overlapping the electronic absorption band of NB, a dual SERRS and MEF performance has been devised under resonant excitation.

- An important part of my thesis was focused on the characterization of single fluorescent nanoprobes through optical microspectroscopy at single nanoparticle level. In this context, we first demonstrated the fluorescence abilities of new hollow gold nanoshells with fluorescent organic dyes in their liquid cores by means of bright field, dark field and fluorescence spectroscopy and microscopy on individual NPs. This is a new kind of hybrid nanoshells exhibiting luminescent properties strong enough to be observed and measured for the first time.

The optimization of these systems and their use as optical sensors, contrast agents for medical imaging or emitting devices might represent attractive work to perform in the future.

- Furthermore, we employ fluorescence microscopy-imaging and spectroscopy to demonstrate the luminescence properties of fluorophore-decorated star and bipiramide-shaped AuNPs. We additionally revealed the self-assembling of bipyramide-like gold nanoparticles in bright shining chain-like nanostructures after conjugation with fluorescent entities.

Future work implies the optimization of the procedure and characterization of samples by transmission electronic microscopy (TEM) and atomic force microscopy (AFM) measurements.

- The final part of my thesis highlight the feasibility of employing surface modified AuNPs in intracellular imaging applications by performing quantitative cellular uptake studies on differently shaped polymer-coated AuNPs. Polyethylene glycol-coated star and bipyramide-shaped AuNPs were successfully uptaken by B16-F10 melanoma cells while the uptake of gold nanospheres (AuNSs) encapsulated in newly synthesized polymeric chains by B16-F10 melanoma and BaF3 lymphoid cells was evaluated as function of colloidal concentration and AuNPs size.

REFERENCES

Bharadwaj P., Deutsch B., Novotny L. *Adv. Opt. Photon*. **2009**, 1, 438–483.

Boca S, Rugina D, Pintea A, Barbu-Tudoran L, Astilean S. *Nanotechnology* **2011**, 22, 055702.

Campion A., Kambhampati P. *Chem. Soc. Rev*. **1998,** 27, 241-250

Huang C. J., Chiu P. H., Wang Y. H., Chen W. R., Meen T. H. *J Electrochem Soc*. **2006**, 153:D129.

Huang X., Neretina S., El-Sayed M. A. *Adv. Mater.* **2009**, 21, 4880–4910.

Lakowicz J. R., *Principles of Fluorescence Spectroscopy*, Third Edition, Springer, **2006.**

Maciejewska W., Polewski K., Grundwald-Wyspiadska M. *Carbohydr. Res*. **1993**, 246, 253-265.

Mie G. *Ann. Phys.* **1908**, 25, 377-445.

Narayanan V. A., Stokes D. L., Vo-Dinht T. J. *Raman Spectrosc.* **1994**, 25, 415-422.

Navarro J. R. G., Manchon D., Lerouge F., Cottancin E., Lermé J., Bonnet C., Chaput F., Mosset A., Pellarin M., Parola S. *Nanotechnology* **2012**, 23, 145707.

Nehl C. L., Liao H., Hafner J. H., *Nano Lett*. **2006**, 6, 683–688.

Sarkar D., Halas N. J. *Phys. Rev. E.* **1997**, 56, 1102-1112.

Shankar S. S., Bhargava S., Sastry M. J Nanosci Nanotechnol. **2005**, 5, 1721-1727.

Tiwari P. M., Vig K., Dennis V. A., Singh S. R. *Nanomaterials* **2011**, 1, 31-63.

Vosgrçne T., Meixner A. J. *Chem Phys Chem* **2005**, 6, 154`-163.

LIST OF PUBLICATIONS

Papers published in ISI Journals:

1. **A. M. Gabudean**, M. Focsan, S. Astilean, *Gold Nanorods Performing as Dual-Modal Nanoprobes via Metal- Enhanced Fluorescence (MEF) and Surface-Enhanced Raman Scattering (SERS)*, Journal of Physical Chemistry, C 116 (2012) 12240-12249. (*IF 4.805*)
2. **A. M. Gabudean**, D. Biro, S. Astilean, *Localized surface plasmon resonance (LSPR) and surface-enhanced Raman scattering (SERS) studies of 4-aminothiophenol adsorption on gold nanorods*, Journal of Molecular Structure, 993(2011) 420-424. (*IF 1.634*)
3. **A. M. Gabudean**, F. Lerouge, T. Gallavardin, M. Iosin, S. Zaiba, O. Maury, P. L. Baldeck, C. Andraud, S. Parola, *Synthesis and optical properties of dyes encapsulated in gold hollow nanoshells*, Optical Materials, 33(2011) 1377-1381. (*IF 2.023*)

Papers published in non ISI Journals:

A. M. Gabudean, D. Biro, S. Astilean, *Synthesis and characterization of silica-encapsulated gold nanorods,* Studia Universitatis "Babeş-Bolyai" Physica, 55, nr. 2, 2010, 33-39.

Submitted papers

A. M. Gabudean, D. Biro, S. Astilean, *Hybrid plasmonic platforms based on silica-encapsulated gold nanorods as effective spectroscopic enhancers for Raman and fluorescence spectroscopy,* submitted to Nanotechnology (2012).

Papers related to my thesis

1. S. Zaiba, F. Lerouge, **A. M. Gabudean**, M. Focsan, J. Lerme, T. Gallavardin, O. Maury, C. Andraud, S. Parola, and P. L. Baldeck, *Transparent Plasmonic Nanocontainers Protect Organic Fluorophores against Photobleaching*, Nano Letters 11 (2011) 2043-2047. (*IF 13.198*)
2. M. Potara, **A. M. Gabudean** and S. Astilean, *Solution-phase, dual LSPR-SERS plasmonic sensors of high sensitivity and stability based on chitosan coated anisotropic silver nanoparticles*, Journal of Materials Chemistry, 21 (2011) 3625-3633. (*IF 5.968*)
3. M. Focsan (Iosin), **A. M. Gabudean**, V. Canpean, D. Maniu and S. Astilean, *Formation of size and shape tunable gold nanoparticles in solution by bio-assisted synthesis with bovine serum albumin in native and denaturated state*, Materials Chemistry and Physics**,** 129 (2011) 939-942. (*IF 2.234*)
4. S. Boca, M. Potara, **A. M. Gabudean**, A. Juhem, P. Baldeck, S. Astilean, *Chitosan-coated triangular silver nanoparticles as a novel class of biocompatible, highly effective photothermal transducers for in vitro cancer cell therapy*, Cancer Letters, 311 (2011) 131-140. (*IF 4.238*)